Articles

Kinetics of Iron(III) Chelation from Polynuclear Oxo-Hydroxy Aggregates by Hydroxamic Acids: Understanding Ferritin Iron(III) Sequestration

David A. Brown,* Kara M. Herlihy,† and Stephen K. O'Shea‡

Department of Chemistry, University College Dublin, Belfield, Dublin 4, Ireland

Received February 8, 1999

The kinetics of the sequestration of iron(III) from the polynuclear iron(III) complex, $[Fe_{11}O_6(OH)_6(O_2CPh)_{15}]\cdot H_2O\cdot 2MeCN$, a possible biomimetic model of ferritin, with a series of 11 primary and secondary hydroxamic acids in dry acetonitrile/dichloromethane solvent mixtures indicates an associative interchange (Ia) mechanism in accordance with the wide variation of $\Delta H^{\ddagger}$ and $\Delta S^{\ddagger}$ within the series. Comparison of the kinetics of this hydroxamic acid series with the simple binuclear iron complex $(NEt_4)_2[Fe_2OC1_6]$ shows that steric effects are considerably more important for the Fe_{11} complex than for the Fe_2 complex. These conclusions, based on kinetics studies, are relevant to the design of chelators for sequestration of iron from ferritin.

Introduction

Ferritin is an important iron storage protein containing an iron core of up to 4500 iron atoms accommodated as a micelle of hydrated ferric oxide of approximate composition $[(FeOOH)_8(FeOPO_3H_2)]$, containing oxo and hydroxo bridges.[1−4] The presence of octahedral iron(III) is confirmed by Mossbauer and electronic absorption spectroscopy and magnetic susceptibility studies.[5−7]

Mammalian apoferritin contains two closely packed polypetide chains (H and L) with channels through which iron may enter or leave the core; although the mechanism of this passage is not clear, the conformational flexibility of the channels is important.[3,7] An understanding of the mobilization of iron from ferritin is important in the design of efficient iron chelators of clinical potential,[8] for example, the use of desferrioxamine-B (DFB) in the treatment of Cooley's anemia.[9,10]

DFB also suppresses iron toxicity and hydroxyl radical formation, and thus, diseases associated with oxygen radical-mediated tissue damage, e.g., neurodegenerative diseases such as Parkinson's and Alzheimer's diseases.[11]

The mechanism of reductive mobilization of iron from ferritin is still unclear[12,13] but has clinical disadvantages, because it may be accompanied by free-radical generation with oxygen (Fenton chemistry) and subsequent tissue damage. Iron(III) chelation, however, has considerable clinical potential. A kinetic approach to understanding the mechanism of direct iron(III) chelation in ferritin is also important, because the thermodynamic properties of the chelating agents do not readily explain the mechanism of chelation.

Previous models of the ferritin core included the polynuclear iron complexes formed by hydrolysis of iron(III) salts, such as that due to Spiro and Saltman with composition $[Fe_4O_3(OH)_4\cdot(NO_3)_3]\cdot 1.5H_2O$[14] and $Na[Fe_4O_4(OH)_{2.6}cit_{0.6}]$, where cit represents the citrate ion formed by deprotonation of the OH group;[15] however, uncertainty in their solution structures mitigates their usefulness as ferritin models.

Recently, a series of well-characterized polynuclear iron complexes, containing aggregates of iron atoms from Fe_6 to Fe_{18} containing bridging carboxylate ligands and oxo and hydroxo bridges, e.g., $[Fe_{11}O_6(OH)_6(O_2CPh)_{15}\cdot H_2O\cdot 2CH_3CN$, have been synthesized by controlled hydrolytic polymerization of simple mononuclear and dinuclear iron anions such as $[FeC1_4]^-$ and $[Fe_2OC1_6]^{2-}$.[16−18] Their mode of formation is formally similar

* Author to whom correspondence should be addressed.
† Present address: Department of Physics, Emory University, Atlanta, GA 30322.
‡ Present address: Department of Plant Pathology, University of California, Riverside, CA 92521.

(1) Waldo, G. S.; Theil, E. C. *Comp. Supramol. Chem.* **1996**, *5*, 65-89.
(2) Harrison, P. M.; Arosio, P. *Biochim. Biophys. Acta* **1996**, *1275*, 161−203.
(3) Pereira, A. S.; Tavares, P.; Lioyd, S. G.; Danger, D.; Edmondson, D. E.; Theil, E. C.; Huynh, B. H. *Biochemistry* **1997**, *36*, 7917−7927.
(4) Thich, J. A.; Ou, C.; Byron, D.; Mustropaolo, D.; Schugar, J.; Powers, D.; Potenza, J. *J. Am. Chem. Soc.* **1976**, *98*, 1425.
(5) Blaise, A.; Chappert, J.; Girardet, J. *C. R. Hebd. Séanc. Acad. Sci.* **1965**, *261*, 2310−2313.
(6) Boas, J. F.; Window, B. *Aust. J. Phys.* **1966**, *19*, 573−576.
(7) Takagi, H.; Dhis, D.; Ha, Y.; Allwell, N. M.; Theil, E. C. *J. Biol. Chem.* **1998**, *273*, 18685−18688.
(8) Brown, D. A.; Chidambaram, M. V. *Metals in Biological Systems*, 14th ed.; Marcel Dekker Inc.: New York, 1982.
(9) Gabutti, V.; Piga, A. *Acta Haematol.* **1996**, *95*, 26−36.
(10) Fosbury, M. J.; Dalton, D. G. *Blood* **1990**, *76*, 435−444.
(11) Raymond, K. N.; Bryan, B. L. *Bioinorganic Chemistry*; 13th ed.; Kluwer Academic Publishers: Norwell, MA, 1995.
(12) Watt, G. D.; Frankel, R. B.; Papaefthymiou, G. C. *Proc. Natl. Acad. Sci. U.S.A.* **1985**, *82*, 3643.
(13) Watt, G.; Jacobs D.; Frankle, R. B. *Proc. Natl. Acad. Sci. U.S.A.* **1988**, *85*, 7457−7461.
(14) Spiro, T. G.; Allerton, S. E.; Rennon, J.; Terzis, A.; Bils, R.; Saltman, P. *J. Am. Chem. Soc.* **1966**, *88*, 2721−2726.
(15) Spiro, T. G.; Pape, L.; Saltman, P. *J. Am. Chem. Soc.* **1967**, *89*, 5555−5559.
(16) Hagen, K. S.; Nair, V. S. *Inorg. Chem.* **1992**, *31*, 4048−4050.
(17) Lippard, S. J. *Chem. Br.* **1986**, *22*, 222−229.
(18) Gorun, S. M.; Papaefthymiou, G. C.; Frankel, R. B.; Lippard, S. J. *J. Am. Chem. Soc.* **1987**, *109*, 3337−3348.

10.1021/ic990158o CCC: $18.00
Published on Web 10/29/1999

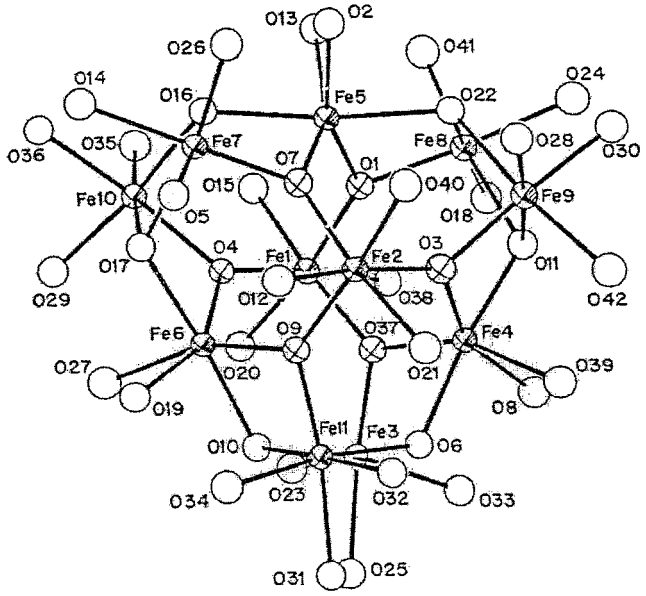

Figure 1. Structure of $[Fe_{11}O_6(OH)_6(O_2CPh)_{15}]$. (All carbon atoms of the benzoate groups are omitted.) Reprinted with permission from *J. Am. Chem. Soc.* **1987**, *109*, 3337−3348. Copyright 1987 American Chemical Society.

to that of the ferritin core, and Lippard and co-workers have suggested the above Fe_{11} complex as a possible precursor in the formation of the iron core.[18]

Because two possible sites of attack by iron chelators on ferritin have been suggested—(1) the ferritin iron core, and (2) the ferrioxidase oxo-bridged dinuclear Fe(III) moiety—ferritin iron mobilization has been modeled in these studies by monitoring the kinetics of the reactions of a series of monohydroxamic acids, R_1CONR_2OH (R_1 = CH_3, C_2H_5, C_5H_{11}, C_8H_{17}; R_2 = H, CH_3, C_6H_5, C_3H_7, 4-C_2H_5-C_6H_4) with both the dinuclear iron complex $(NEt_4)_2[Fe_2OC1_6]$ and the polynuclear complex $[Fe_{11}O_6(OH)_6(O_2CPh)_{15}]\cdot H_2O\cdot 2CH_3CN$ (Figure 1).

Experimental Section

General Considerations. All solvents were dried and distilled prior to use.[19] Reagents and glassware were at all times kept moisture-free, as any absorbed moisture could hydrolyze reactants and thus complicate kinetic measurements. Dichloromethane and acetonitrile were dried by refluxing over CaH_2 and self-indicating $CaSO_4$, respectively. The solvents were degassed and stored over hot, dried molecular sieves. Immediately prior to use, the solvents were mixed in a 1:1 ratio, calculated by weight. To prevent decomposition of iron compounds in solution, all solutions were prepared and used in situ. Prior to injection of the solutions, the injection apparatus, mixing cells, tubing, and so forth were flushed through with acetonitrile containing self-indicating $CaSO_4$ to ensure moisture-free conditions. All anaerobic manipulations were carried out using standard Schlenck techniques. Infrared spectra were obtained using a Perkin-Elmer 1720FT spectrometer linked to a 3700 data station. UV/visible spectra were

measured in acetonitrile and dichloromethane (1:1weight ratio mixture) on a Perkin-Elmer Lambda 6 spectrometer. NMR spectra were recorded on a JEOL JNM-GX270FT NMR spectrometer using a range of deuterated solvents and TMS as a reference. Analyses of reagents, prior to use, were performed by the Microanalytical Unit of the Chemical Services Unit of University College Dublin.

Preparation of Primary Hydroxamic Acids. The alkyl monohydroxamic acids were prepared as described previously.[20]

Preparation of Secondary Hydroxamic Acids. *N*-Methyl Hydroxamic Acids. *N*-Methyl hydroxylamine (8.35 g, 0.1 M) was stirred in dry ethanol (60 mL) with Na_2CO_3 for 1 h. The solution was cooled, and acetyl chloride (7.11 mL, 0.1 M) was added dropwise over 1 h with stirring. The solution was then filtered free of NaCl and evaporated under reduced pressure at room temperature. A clear yellow oil was obtained. This was distilled using a Kugel−Rohr under reduced pressure (bp 74−76 °C/0.8 mm). This step was important because it allowed complete removal of trace acid chlorides, esters, and so forth. The oil was freeze-dried for 2 days to obtain an analytically pure product (see Supporting Information).

N-Methyl *n*-hexano hydroxamic acid was also prepared in a similar fashion, employing hexanoyl chloride in place of acetyl chloride.

***N*-Isopropyl Hydroxamic Acids.** A similar procedure was employed to prepare *N*-isopropyl *n*-hexano and *N*-isopropyl acetohydroxamic acids. *N*-Isopropyl hydroxylamine was freeze-dried prior to use, and the products were recrystallized using pentane to give white, analytically pure crystals.

N-Phenyl hydroxylamine and the *N*-phenyl substituted hydroxamic acids were synthesized using methods previously reported by Brink and Crumbliss.[21]

Preparation of μ-Oxo Iron(III) Species. Several preparations of the basic μ-oxo unit $[Fe_2OC_6]^{2-}$ were available; however, that of W. H. Armstrong and S. J. Lippard proved to be the most convenient and efficient method.[22]

$[Fe_{11}O_6(OH)_6(O_2CPh)_{15}]\cdot H_2O\cdot 2MeCN$ was prepared as described in ref 18.

Preparation of Deuterated *N*-Phenyl Acetohydroxamic Acid. *N*-Phenyl acetohydroxamic acid (5 g) was dissolved in an excess of D_2O (99.95%, D) to which a trace amount of purified triethylamine had been added. The solvent was then removed by repetitive freeze-drying. Standard Schlenck procedures were followed throughout and during all subsequent manipulations employing this compound.

Stopped-Flow Kinetic Experiments. Stopped-flow experiments were executed using a Carl Zeiss M4G11 (3293-3) apparatus. The temperature of the cell and injection platform were maintained using a Towson and Mercer thermostat and pump. Kinetic results were monitored at 426 nm using a Hameg digital storage oscilloscope (HM205-2) and the results stored on a data lab transient recorder (DL905) which was interfaced (specifically assembled) with a 286/SX-25 PC. Data were collected by custom-designed software at a sampling rate such that approximately 3000 points were acquired over the course of the reaction with a linear time base. All kinetic runs were made in dry acetonetrile and dichloromethane (1:1 weight ratio mixture).

Pseudo-first-order kinetic data, used to determine rate constants and activation parameters for the reaction of both Fe_2 and Fe_{11} complexes, were generated by flowing hydroxamic acid solutions over the concentration range, 0.01−0.0025 M with 0.0005 M iron solution, under variable temperature conditions. Continuous scan experiments showed no evidence for formation of intermediate species, and provided the ligand-to-iron concentration ratio is maintained greater than 33.1, the tris complex FeA_3 (λ_{max}, 426 nm) is the sole product. On reducing this ratio to 11:1, some bis complex (λ_{max}, 465 nm) was formed, but no evidence was obtained for formation of the mono complex (λ_{max}, 501 nm). Moreover, in the case of the 33:1 concentration ratio, the spectra show a distinct isobestic point, in accord with clean reactant conversion. These results imply that preequilibrium ternary complexes are not formed; however, solubility factors limited variation of [HA], thereby precluding observation of saturation kinetics. Finally, the ^1H NMR spectra of the HA ligands used in this study gave no evidence for proton loss in either CD_2Cl_2 or CD_3CN.

Results

The kinetic results for the range of hydroxamic acids studied with both Fe_2 and Fe_{11} complexes, together with calculated

(19) Perrin, D. D.; Armaregon, W. L. F. *Purification of Laboratory Chemicals*, 3rd ed.; Oxford Press: Pergamon Press Ltd., U.K., 1988.
(20) Brown, D. A.; Roche, A. L. *Inorg. Chem* **1983**, *22*, 2199.
(21) Crumbliss, A. L.; Brink, C. P *J. Org. Chem.* **1982**, *47*, 1171.
(22) Armstrong, W. H.; Lippard, S. *J. Inorg. Chem.* **1985**, *24*, 981

Table 1. Kinetic Results for the Reaction of $(Et_4N)_2[Fe_2OCl_6]$ with a Series of Monohydroxamic Acids[a]

hydroxamic acid	R_1, R_2	rate const (s^{-1} mol^{-1}), 25 °C	$\Delta H^{\ddagger}$ (kJ mol^{-1})	$\Delta S^{\ddagger}$ (J K^{-1} mol^{-1})
aceto	CH_3, H	$(1.90 \pm 0.10) \times 10^3$	26.1 ± 2.9	-94.6 ± 5.5
propano HA	C_2H_5, H	$(2.33 \pm 0.10) \times 10^3$	34.6 ± 1.2	-64.5 ± 2.0
hexano HA	C_5H_{11}, H	$(2.58 \pm 0.13) \times 10^3$	37.3 ± 1.2	-54.6 ± 1.6
N-methylaceto HA	CH_3, CH_3	$(1.67 \pm 0.07) \times 10^3$	17.9 ± 0.9	-123.7 ± 3.3
N-phenylaceto HA	CH_3, C_6H_5	$(1.13 \pm 0.07) \times 10^3$	31.3 ± 1.9	-81.7 ± 4.6
N-isopropylaceto HA	CH_3, C_3H_7	$(1.14 \pm 0.06) \times 10^3$	28.2 ± 2.0	-91.8 ± 6.0
N-hexano HA	C_5H_{11}, CH_3	$(1.14 \pm 0.03) \times 10^3$	23.5 ± 1.50	-107.6 ± 6.0
N-phenylhexano HA	C_5H_{11}, C_6H_5	$(0.726 \pm 0.04) \times 10^3$	54.4 ± 4.0	-7.65 ± 0.5

[a] Solvent: CH_3CN/CH_2Cl_2 (1:1). Concentration range of excess reagent: 0.01−0.0025 M

Table 2. Kinetic Results for the Reaction of $[Fe_{11}O_6(OH)_6(O_2CPh)_{15}]\cdot H_2O\cdot 2MeCN$ with a Series of Monohydroxamic Acids[a]

hydroxamic acid	R_1, R_2	rate const (s^{-1} mol^{-1}), 30 °C	$\Delta H^{\ddagger}$ (kJ mol^{-1})	$\Delta S^{\ddagger}$ (J K^{-1} mol^{-1})
aceto	CH_3, H	41.1 ± 2.1	25.5 ± 1.7	-130.0 ± 5.5
propano HA	C_2H_5, H	30.8 ± 1.5	34.7 ± 2.6	-102.2 ± 6.4
hexano HA	C_5H_{11}, H	7.91 ± 0.4	59.4 ± 0.7	-32.3 ± 2.5
nonano Ha	C_8H_{17}, H	7.86 ± 0.4	60.3 ± 0.9	-29.4 ± 0.93
N-methylaceto HA	CH_3, CH_3	3.52 ± 2.5	63.4 ± 4.0	-25.6 ± 2.0
N-phenylaceto HA	CH_3, C_6H_5	1.18 ± 0.06	64.8 ± 3.8	-29.7 ± 3.4
N-isopropylaceto HA	CH_3, C_3H_7	1.07 ± 0.05	66.3 ± 3.0	-26.1 ± 1.5
N-methylhexano HA	C_5H_{11}, CH_3	1.34 ± 0.07	60.2 ± 2.1	-44.3 ± 2.0
N-phenylhexano HA	C_5H_{11}, C_6H_5	1.06 ± 0.05	68.7 ± 3.2	-17.8 ± 1.6
N-(4-Et)-phenylhexano HA	C_5H_{11}, 4-C_2H_5-C_6H_4	0.502 ± 0.05	70.6 ± 1.1	-18.2 ± 2.0
N-isopropylhexano HA	C_5H_{11}, C_3H_7	0.542 ± 0.03	69.9 ± 2.8	-19.7 ± 1.0

[a] Solvents: CH_3CN/CH_2Cl_2 (1:1). Concentration range of excess reagent: 0.01−0.0025 M

enthalpies and entropies of activation, $\Delta H^{\ddagger}$ and $\Delta S^{\ddagger}$, are given in Tables 1 and 2, respectively, and may be summarized as follows.

Fe_2 Series (Table 1). For the primary hydroxamic acids, $\Delta H^{\ddagger}$ increases in the series aceto < propano < hexano, while $\Delta S^{\ddagger}$ becomes less negative in this series. For the secondary hydroxamic acids, $\Delta H^{\ddagger}$ increases in the series *N*-methylaceto < *N*-methylhexano < *N*-isopropylaceto < *N*-phenylaceto ≪ *N*-phenylhexano, while $\Delta S^{\ddagger}$ becomes less negative in this series. Comparing primary and secondary hydroxamic acids:$\Delta H^{\ddagger}$ lies in the sequence; *N*-methylaceto < aceto; *N*-methylhexano < hexano, while $\Delta S^{\ddagger}$ becomes less negative in these sequences.

Fe_{11} Series (Table 2). For the primary hydroxamic acids, $\Delta H^{\ddagger}$ lies in the same sequence as above: aceto < propano < hexano, while again $\Delta S^{\ddagger}$ becomes less negative in this sequence. For the secondary hydroxamic acids, $\Delta H^{\ddagger}$ increases in the series *N*-methylhexano < *N*-methylaceto < *N*-phenylaceto < *N*-isopropylaceto < *N*-phenylhexano < *N*-isopropylhexano, while $\Delta S^{\ddagger}$ becomes less negative in the sequence *N*-methylhexano < *N*-phenylaceto < *N*-isopropylaceto < *N*-methylaceto < *N*-phenylhexano.

Discussion

The results in Tables 1 and 2 give support for the operation of an associative interchange (Ia) mechanism for these reactions for the following reasons. First, there is a 100-fold variation in the rate constants at 30 °C, with variation in hydroxamic acid for the Fe_{11} complex. Second, there is significant variation in $\Delta H^{\ddagger}$, with variation in hydroxamic acid for both the Fe_2 and Fe_{11} complexes. Finally, in all cases $\Delta S^{\ddagger}$ is negative, as is expected for an associative mechanism. These general observations showing large variations with entering groups are supportive of the I_a mechanism. It should also be noted that the rate constants for the Fe_2 complex are about 100−1000 times greater than for the F_{11} complex, in accordance with much greater steric effects for the latter system. Detailed comments on the activation parameters are as follows.

Fe_2 (Series). (a) The above order of $\Delta H^{\ddagger}$ for primary hydroxamic acids reflects a decrease in electron density at the carbonyl oxygen atom as the methyl group is replaced by longer chain groups. At the same time, $\Delta S^{\ddagger}$ becomes less negative, indicating greater steric effects.

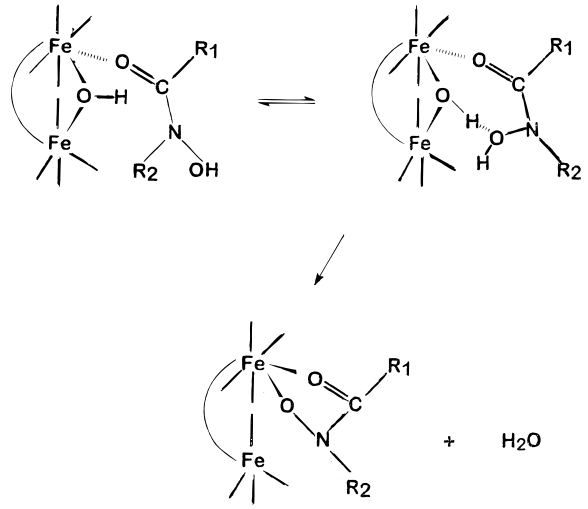

Figure 2. Proposed mechanism for formation of the transition state.

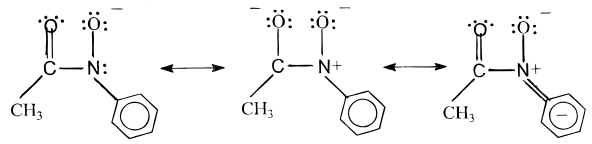

Figure 3. Resonance structures for *N*-phenylaceto hydroxamic acids ($R_1 = CH_3$; $R_2 = C_6H_5$).

(b) In the sequence of the secondary hydroxamic acids, electron-donating substituents on the N atom (R_2 substituent) cause delocalization of the N atom lone pair of electrons into the C−N bond, which in turn increases the electron density at the carbonyl oxygen atom (Figure 3), resulting in increased C−O−Fe interactions and therefore lower $\Delta H^{\ddagger}$ values compared to those of the corresponding primary acid and also within the sequence for secondary acids, in order of increasing donor strength of R_2; for example, $\Delta H^{\ddagger}$ for *N*-methylaceto is less than

that for *N*-isopropylaceto, whereas *N*-phenylaceto > aceto and *N*-phenylhexano > hexano. In the case of these *N*-phenyl hydroxamic acids, the trend in $\Delta H^{\ddagger}$ is the opposite of that observed for the *N*-methyl cases, reflecting the electron-accepting nature of the phenyl group. Similar trends have been observed by Crumbliss and co-workers in their study of complexation of high-spin aqueous Fe(III) by a series of hydroxamic acids.[23,24] The greater effect of R_2 occurs because both resonance and inductance effects arise for the R_2 substituent on the nitrogen atom (Figure 3).

(c) The entropies of activation ($\Delta S^{\ddagger}$) lie in the following sequence (Table 1): *N*-phenylhexano > hexano > propano > *N*-phenylaceto > *N*-isopropylaceto > *N*-methylhexano > *N*-methylaceto, with *N*-methyl aceto having the most negative $\Delta S^{\ddagger}$ value and thus the most ordered and tightly bound transition state. Variation in R_2 causes both electronic and steric effects which are reflected in the $\Delta S^{\ddagger}$ values. For example, in *N*-isopropylaceto, the *N*-isopropyl group exerts an electronic effect which is balanced by its steric effect with $\Delta H^{\ddagger} = 28.2$ kJ mol^{-1} and $\Delta S^{\ddagger} = -91.8$ J K^{-1} mol^{-1} compared to the corresponding *N*-methyl case with $\Delta H^{\ddagger} = 17.9$ kJ mol^{-1} and $\Delta S^{\ddagger} = -123.7$ J K^{-1} mol^{-1}. This effect probably arises from the higher E→Z rotational barrier for *N*-isopropylaceto compared to that of *N*-methylaceto, which means it will have more difficulty in rotating to the Z-conformation required by the transition state shown in Figure 2.

Comparison of Fe_2 and Fe_{11} series. (a) For the primary hydroxamic acid series, $\Delta H^{\ddagger}$ increases in the series methyl < ethyl < hexano with very similar values for aceto and propano in both the Fe_2 and the Fe_{11} series; however, the value of $\Delta H^{\ddagger}$ for hexano is considerably greater for Fe_{11} than for the Fe_2 case [$\Delta H^{\ddagger} = 59.4$ (Fe_{11}) compared to $\Delta H^{\ddagger} = 37.3$ (Fe_2)], suggesting that the longer chain acid encounters a larger steric effect for the Fe_{11} system than the short chain acids. (b) For the secondary hydroxamic acid series, $\Delta H^{\ddagger}$ increases in a series similar to the Fe_2 series but with some changes in order; for example, in the Fe_2 series: $\Delta H^{\ddagger}$ (*N*-methylhexano) < $\Delta H^{\ddagger}$ (aceto); whereas for the Fe_{11} complex $\Delta H^{\ddagger}$ (*N*-methylhexano) > $\Delta H^{\ddagger}$ (aceto), reflecting the greater impact of increasing chain length of the substituent R_1 in the case of the Fe_{11}complex compared to that in the Fe_2 series (see below). The $\Delta S^{\ddagger}$ values support this argument for each given ligand because the steric effects are greater in the Fe_{11} series than in the Fe_2 series (tables 1 and 2), consistent with the idea that the benzoate bridges in the Fe_{11} complex crowd the oxo bridges, the point of ligand attack (Figure 2), and so inhibit rotation of the E→Z conformer of the attacking hydroxamic acid ligand. Increasing chain length of the R_1 substituent has a greater retarding effect for the Fe_{11} series than for the Fe_2 series.

Thus, for the Fe_{11} complex, $\Delta H^{\ddagger}$ (hexano) (59.4 kJ mol^{-1}) > $\Delta H^{\ddagger}$ (aceto) (25.5 kJ mol^{-1}) and $\Delta S^{\ddagger}$ (hexano) (−32.3 J K^{-1} mol^{-1}) > $\Delta S^{\ddagger}$ (aceto) (−130.0 J K^{-1} mol^{-1}), whereas for the Fe_2 complex, $\Delta H^{\ddagger}$ (hexano) (37.3 kJ mol^{-1}) > $\Delta H^{\ddagger}$ (aceto) (26.1 kJ mol^{-1}) and $\Delta S^{\ddagger}$ (hexano) (−54.6 J K^{-1} mol^{-1}) > $\Delta S^{\ddagger}$ (aceto) (−94.6 J K^{-1} mol^{-1}).

Isokinetic Plots. The plots of $\Delta H^{\ddagger}$ versus $\Delta S^{\ddagger}$ for the reaction of the Fe_2 and Fe_{11} complexes with eight hydroxamic acids used in this study are shown in Figure 4. The slopes (β values) of the series Fe_{11}, $\beta = 0.32$ compare well with the β value of 0.328 reported by Crumbliss et al.[25] for the reactions of a similar series of substituted hydroxamic acids with aqueous iron(III). The wide range of $\Delta H^{\ddagger}$ and $\Delta S^{\ddagger}$ values within these series of hydroxamic acids is good evidence for an associative mechanism as shown in Figure 2 and similarly assigned by Crumbliss as an associative interchange (Ia) mechanism in his studies with aqueous iron(III). However, it should be noted that the order of substituent effects sometimes changes between the Fe_2 and Fe_{11} systems (Figure 4). We consider this to be a result of steric effects predominating in the Fe_{11} series, although a change of mechanism between the Fe_{11} and Fe_2 series cannot be excluded.

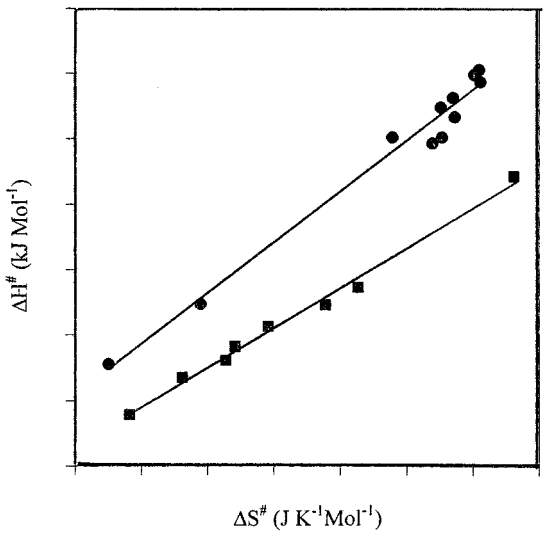

Figure 4. Isokinetic relationship in Fe_{11} and Fe_2 series. ●: Fe_{11} series (isokinetic temperature, 0.38 ± 0.02 K). ■: Fe_2 series (isokinetic temperature, 0.31 ± 0.01 K).

Isotope Effects. The transition state shown in Figure 2, which involves initial attack by a carbonyl oxygen atom at an iron center rather than attack by hydrogen bonding of the O−H of the hydroxamic acid ligand to an oxo bridge, would not be expected to show a significant kinetic isotope effect. The rate ratio (k_H/k_D) of 1.40 obtained for the reaction between the Fe_{11} complex and deuterated *N*-phenyl hydroxamic acid is in reasonable agreement with the suggested mechanism but does not exclude a dissociative mechanism.

Conclusions

Based on the above observations, an associative interchange (Ia) mechanism is suggested for the reactions of a series of hydroxamic acids with Fe_2 and Fe_{11} complexes. These reactions involve an initial attack on an iron center by the hydroxamic carbonyl oxygen, followed by rotation of the C−N bond so that the hydroxamic hydroxyl group may hydrogen-bond to the oxo bridge, followed by a ring closure to form a monohydroxamate complex with displacement of the benzoate bridges (Figure 2). Such attack involving replacement of bridging carboxylate groups in dinuclear complexes such as [$Ni_2(OAc)_4(\mu$-$H_2O)$-$(tmen)_2$] by hydroxamate has recently been shown to be facile.[26] This cleavage exposes the polymeric iron structure leading to breakage of the μ3 and μ2 oxo bridges and rapid attack at the resulting coordinately unsaturated iron centers by a large excess of hydroxamic acid.

(23) Tyler Caudle, M.; Crumbliss, A. L. *Inorg. Chem.* **1994**, *33*, 4077−4085.
(24) Crumbliss, A. L. *CRC Handbook of Microbial Iron Chelates*, 7th ed.; CRC Press: New York, 1991.
(25) Brink, C. P.; Crumbliss, A. L. *Inorg. Chem.* **1984**, *23*, 4708.
(26) Arnold, M.; Brown, D. A.; Deeg, O.; Errington, W.; Haase, W.; Herlihy, K.; Kemp, T. J.; Nimir, H.; Werner, R. *Inorg. Chem.* **1998**, *37*, 2920.

As discussed in the Introduction, the design of efficient iron chelators for mobilizing iron from ferritin is an important therapeutic goal. Using the Fe_{11} complex as a biomimetic model for ferritin, the above kinetic studies have shown clearly the importance of steric factors as well as electronic factors in determining the ability of a wide range of primary and secondary hydroxamic acids to mobilize iron from this model. Short-chain primary hydroxamic acids are the most efficient chelators, and although the electronic effects of N-substituents may assist energetically, those effects are largely outweighed by steric inhibition. These conclusions—based on kinetic data obtained, by necessity, in dry acetonitrile/dichloromethane solutions—are likely to apply generally to polar solvents. In view of the importance of kinetic factors in understanding the mechanism of iron sequestration from ferritin, the present work provides a clear structural indication for chelator design based on detailed kinetic studies of the reactions of well-characterized polynuclear iron models of ferritin with hydroxamic acids.

Acknowledgment. Professor E. Farkas, University of Debrecen, Hungary; Professor H. W. Sidebottom, University College Dublin, Ireland; and Professor A. L. Crumbliss, Duke University, North Carolina, are gratefully acknowledged for their helpful comments and suggestions. Support from the EUCOST program, project D8/0010/97, is also acknowledged.

Supporting Information Available: Tables giving analytical kinetic (rate constants, Arrhenius and Eyring plots) and isotopic exchange results (two tables and nine plots); UV-visible spectra of complex formation (three figures). This material is available free of charge via the Internet at http://pubs.acs.org.

IC990158O